

IDENTIFYING SPATIAL PATTERNS OF STORM DRIVEN FLOODING AND EROSION
AT NELSON LAGOON, ALASKA

By

Reyce C. Bogardus, B.S.

A Thesis Submitted in Partial Fulfillment of the Requirements

for the Degree of

Master of Science

in

Geosciences

University of Alaska Fairbanks

May 2021

APPROVED:

Chris Maio, Committee Chair

Daniel Mann, Committee Member

Jacquelyn Overbeck, Committee Member

Paul McCarthy, Chair

Department of Geosciences

Kinchel Doerner, Dean

College of Natural Sciences and Mathematics

Richard Collins, *Director of the Graduate School*

ABSTRACT

This project quantifies localized potential for shoreline change and flooding at Nelson Lagoon, a small fishing community located on the Bering Sea coast of the Alaska Peninsula. The overall goal of this project is to generate societally relevant and locally applicable map and data products through synergistic relationships with federal, state, private, tribal, and public partners. This project intends to substantiate anecdotal observations by local residents, with the ultimate goal of informing erosion and flooding mitigation efforts moving forward.

Long-term trends of shoreline change were measured using multi-temporal orthorectified aerial imagery between 1983 and 2019, while annual changes in shoreline morphology were measured via cross-shore elevation profiles using a survey grade Real-time-Kinematic Global Navigational Satellite System (RTK-GNSS). Shoreline positions were extrapolated using linear regression techniques. A digital surface model (DSM) of the community was derived using Structure-from-Motion (SfM) with >2,400 aerial images collected with an Unmanned Aerial Vehicle (UAV) and used to assess flooding vulnerability after being geodetically referenced and related to a local tidal datum computed by this project. New and existing topographic and bathymetric datasets were compiled and refined into a 6,000 km² topobathymetric “seamless elevation” model of the Nelson Lagoon area, over which storm-tide induced currents were simulated using Delft3D FM Suite HMWQ.

Remote sensing records indicate that the Nelson Lagoon spit elongated by more than 800 m and narrowed with an average Net Shoreline Movement (NSM) of -16.9 m between 1983 and 2019 (distal end not included). Though, NSM values show high variability ($\sigma = 21.9$ m) and the lagoon and seaward sides of the spit are exhibiting very different erosional regimes. On both sides of the spit, episodes of rapid erosion mainly occurred during high storm-tide events that coincided with significant wave action. For this reason, the long-term erosion rates ultimately reflect the combined erosional impact of just a few storm events. Sand dunes in the supratidal zone on both sides of the spit are eroding at the vegetation line while the dune face retreats landward. By assessing erosion and flooding vulnerabilities for the Nelson Lagoon community, this study adds to an ever-growing database of such assessments statewide; which, ultimately, advance our understanding of regional coastal change in a shifting environment.

[This page is intentionally left blank]

PREVIEW

TABLE OF CONTENTS

	Page
ABSTRACT	i
LIST OF FIGURES	v
LIST OF TABLES	v
LIST OF APPENDICES	x
LIST OF ABBREVIATIONS	xi
ACKNOWLEDGEMENTS	xiv
CHAPTER 1 INTRODUCTION	1
1.1 Introduction	1
1.2 Research Question and Objectives	3
1.3 Background	3
1.3.1 Regional Storm Regime	3
1.3.2 Regional Sea Ice Regime.....	6
1.3.3 Erosion / Flooding	9
1.4 Study Site	12
1.4.1 Demographics.....	12
1.4.2 Economy	12
1.4.3 Transportation.....	13
1.4.4 Infrastructure	13
1.5 Environmental Setting.....	15
1.5.1 Geography [Bristol Bay Region / Alaska Peninsula]	15
1.5.2 Geologic Setting	18
1.5.3 Oceanographic Setting.....	20
1.5.4 Climatological Setting	22
1.6 Previous Work at Nelson Lagoon	26
CHAPTER 2 METHODS	27
2.1 Overview	27
2.2 Quantifying Patterns of Erosion Vulnerability.....	27
2.2.1 Shoreline Change Analysis.....	27

2.2.2 Cross-shore Elevation Profiles	31
2.3 Quantifying Patterns of Flooding Vulnerability.....	33
2.3.1 Single-Value Threshold Map.....	33
2.3.2 Delft3D FM Model.....	37
2.4 Assessing At-risk Infrastructure.....	44
CHAPTER 3 RESULTS.....	45
3.1 Overview	45
3.2 Patterns of Erosion Vulnerability.....	45
3.3 Patterns of Flooding Vulnerability.....	53
3.3.1 Single Value Threshold Map.....	53
3.3.2 Delft3D FM Computational Setup	55
CHAPTER 4 DISCUSSION	57
4.1 Overview	58
4.2 Spatial Patterns of Vulnerability and Implications	58
4.2.1 Study Limitations	61
4.2.2 Areas of Greatest Concern.....	63
4.3 Compounding Factors	67
4.3.1 Sea Level Rise	67
4.3.2 Coseismic and Interseismic Deformation.....	70
4.4 Broader Impacts	74
4.5 Future Work	76
CHAPTER 5 CONCLUSION.....	77
5.1 Application of Surveyed & Remotely Sensed Data	77
5.2 Community Threat Assessment	77
5.3 Coastal Resiliency of Nelson Lagoon.....	78
LITERATURE CITED	79

LIST OF FIGURES

	Page
Figure 1. Study site map of the Native Village of Nelson Lagoon.....	2
Figure 2. Storm track density climatology in the North Pacific from 1948/49 to 2008.	4
Figure 3. Plot showing the last hundred years of the mean winter (DJFM) North Pacific index, Pacific Decadal Oscillation Index, and surface air temperature in the Bering Sea.	6
Figure 4. Megatransect of sea-ice concentrations for the month of March between 1850 and 2018 compiled from the Alaska Ocean Observatory Network (AOOS) Sea Ice Atlas. ...	8
Figure 5. Diagram showing the various components of Total Water Level (TWL); waves, tides, and nontidal residuals.	11
Figure 6. Map showing the building and utility infrastructure of Nelson Lagoon.	14
Figure 7. Cross-section of the Nelson Lagoon spit where the residential area is located.....	16
Figure 8. Cross-shore photograph taken in 2019 on the Bering Sea-side of the Nelson Lagoon spit near the community.....	17
Figure 9. Generalized surficial geology of the Nelson Lagoon area (red star).....	19
Figure 10. Graphic representation of the relative strength of component marine energy in Bristol Bay, and the characteristic barrier morphologies.....	20
Figure 11. Various tidal datums computed using data over a 6-month period for Nelson Lagoon with JOA Surveys, LLC tidal datum tool.	21
Figure 12. Wave roses for each month averaged over 29 years (1985-2014) from digital buoy WIS station 82289 (56.25°, -161.25°).	23
Figure 13. Mean fall temperatures at Nelson Lagoon’s airstrip between 2010 and 2019 compiled from the Automated Surface Observing System (ASOS).....	24
Figure 14. Wind roses for each month averaged over 9 years of observations (2010 - 2019) from the ASOS-integrated meteorological station at the Nelson Lagoon airport.....	25

Figure 15. Map displaying the digital transects (thin black line) that were caste from a base line (thick black line) across the digitized shorelines.....	28
Figure 16. Map showing the location of each cross-shore elevation profile (black line) and community infrastructure (red box).	31
Figure 17. Map showing the location of CORS stations used to refine the base station coordinates.....	33
Figure 18. Map showing the locations of control and validations points used to process the UAV-derived DSM.	35
Figure 19. Plot of the covariance between the elevation values of the refined DSM surface (y-axis) and GNSS points used to validate the model (x-axis).	36
Figure 20. Map showing the D-FLOW model domain (red line) and bathymetry.....	40
Figure 21. Plot of the covariance between the elevation values of the IfSAR DTM surface (y-axis) and GNSS points used to validate the model (x-axis).	41
Figure 22. Map showing the bathymetry of the Nelson Lagoon area on a structured Delft3D grid.....	43
Figure 23. Map showing the Net Shoreline Movement (NSM) computed by the historic shoreline change assessment.	46
Figure 24. Map showing the projected shoreline positions (2029 and 2039) across section A from the 2019 shoreline.....	47
Figure 25. Cross-shore elevation profiles from 2018 and 2019 within section A.	48
Figure 26. Map showing the projected shoreline positions (2029 and 2039) across section B from the 2019 shoreline.	49
Figure 27. Cross-shore elevation profiles from 2014, 2015, 2018, and 2019 within section B.	49
Figure 28. Map showing the projected shoreline positions (2029 and 2039) across section C from the 2019 shoreline.	50

Figure 29. Cross-shore elevation profiles from 2018 and 2019 within section C.	51
Figure 30. Map showing the projected shoreline positions (2029 and 2039) across section D from the 2019 shoreline.	52
Figure 31. Cross-shore elevation profiles from 2014, 2015, 2018, and 2019 within section D.	52
Figure 32. Single value threshold flood risk map of the Nelson Lagoon residential area, color coded based off elevation in meters above mean high water.	54
Figure 33. Graphic showing insets of the larger SVTM where photographs of high storm-tide events have been captured.	55
Figure 34. 3D rendering of the produced topobathymetric elevation model, shown in Google Earth.	56
Figure 35. Diagrams showing the depth averaged velocity of the water column in six-hour increments over the temporal domain (11/11/11 0:00 to 11/13/11/ 0:00).	57
Figure 36. Cross-shore elevation profiles from the ocean side (top) and lagoon-side (bottom) of the Nelson Lagoon spit.	59
Figure 37. UAV imagery showing the remnants of overwash deposits along the ocean side of the Nelson Lagoon spit.	60
Figure 38. Tsunami hazard map of Nelson Lagoon, produced by the Alaska Earthquake Center for the Alaska Department of Geologic and Geophysical Surveys (from Suleimani et al., 2020).	63
Figure 39. Foredune breach along the ocean shoreline fronting the community airstrip.	64
Figure 40. A flooded road near the retaining wall on the east side of the community.	65
Figure 41. Seawall and sediment containers in place along the lagoon coastline of the community.	65
Figure 42. Photograph taken from the solid waste disposal site looking towards the community on the ocean side of the spit.	66

Figure 43. Photograph showing remnants of an overwash and flooding event at the access road from the beach to the solid waste disposal site, which can be seen to the left.	67
Figure 44. Plot showing the monthly mean sea level without the regular seasonal fluctuations from Port Moller Station.	68
Figure 45. Flowchart illustrating how wetland loss leads to increasing tidal prism, larger tidal inlets, and enlarging ebb-tidal deltas.	70
Figure 46. Map showing the location of the Shumigan Gap and all large recent earthquakes along the Aleutian Subduction Zone, including the magnitude 7.8 in the Shumagin Gap that occurred July 21, 2020.	71
Figure 47. Processed daily position time series of GNSS station AC41 Port Moller, AK between 2006 and 2020, from the UNAVCO Data Center.	73
Figure B.1 Elevation profile A.	99
Figure B.2 Elevation profile B.	99
Figure B.3 Elevation profile C.	100
Figure B.4 Elevation profile D.	100
Figure B.5 Elevation profile E.	101
Figure B.6 Elevation profile F.	101
Figure B.7 Elevation profile G.	102
Figure B.8 Elevation profile H.	102
Figure B.9 Elevation profile I.	103
Figure B.10 Elevation profile J.	103
Figure B.11 Elevation profile K.	104
Figure B.12 Elevation profile L.	104

Figure B.13 Elevation profile M.....	105
Figure B.14 Elevation profile N.....	105
Figure B.15 Elevation profile O.....	106
Figure B.16 Elevation profile P	106
Figure B.17 Elevation profile Q.....	107
Figure B.18 Elevation profile R.....	107
Figure B.19 Elevation profile S	108
Figure B.20 Elevation profile T	108
Figure B.21 Elevation profile U.....	109
Figure B.22 Elevation profile V.....	109
Figure B.23 Elevation profile W.....	110
Figure B.24 Elevation profile X.....	110
Figure B.25 Elevation profile Y.....	111
Figure B.26 Elevation profile Z.....	111
Figure B.27 Elevation profile Aa.....	112
Figure B.28 Elevation profile Bb.....	112
Figure B.29 Elevation profile Cc	113
Figure B.30 Elevation profile Dd.....	113

LIST OF TABLES

	Page
Table 1. Summary of aerial imagery used for shoreline delineation.	27
Table 2. Vegline uncertainty values with total uncertainty (U_t) bolded (after Buzard, 2007)	30
Table 3. Overview of average RTK vector precision characteristics by survey category	32
Table 4. Overview of the UAV surveys used to construct the Digital Surface Model (DSM)	34
Table 5. Overview of the compiled datasets/surveys used to construct the seamless elevation model upon which the computational grid was derived.....	39
Table 6. The parameter settings of the D-FLOW run.....	44
Table 7. Average shoreline change analysis results by shoreline section.....	47
Table 8. Overview of the building elevations in Nelson Lagoon, organized by infrastructure class.....	53
Table A.1 Error between GCPs and the point cloud in the X, Y, and Z dimensions	96

LIST OF APPENDICES

	Page
Appendix A. GCP Processing Report.....	95
Appendix B. Cross-shore Elevation Profiles	100

LIST OF ABBREVIATIONS

AA	Arctic Amplification
ACGL	Arctic Coastal Geoscience Laboratory
ADEC	Alaska Department of Environmental Conservation
ADLWD	Alaska Department of Labor and Workforce Development
ADVs	Acoustic Doppler Velocimeters
AFZ	Arctic Frontal Zone
AGU	American Geophysical Union
AHAP	Alaska High Altitude Photography
AIJ	Alaska Institute for Justice
ANTHC	Alaska Native Tribal Health Consortium
AOOS	Alaska Ocean Observing System
ASG	Alaska Sea Grant
ASOS	Automated Surface Observing System
CIFAR	Cooperative Institute for Alaska Research
DCRA	Division of Community and Regional Affairs
DGGS	Department of Geologic and Geophysical Surveys
DLG	Dillingham
DSAS	Digital Shoreline Analysis System
DSM	Digital Surface Model
DTM	Digital Terrain Model
EPR	End Point Rate
ESRI	Environmental Systems Research Institute
FEMA	Federal Emergency Management Agency
FM	Flexible Mesh
GAO	Government Accountability Office
GCP	Ground Control Point

GIS	Geographic Information System
GLONASS	Global Orbiting Navigation Satellite System
GNSS	Global Navigation Satellite System
GSA	Geological Society of America
IfSAR	Interferometric Synthetic Aperture Radar
MHW	Mean High Water
MLLW	Mean Lower Low Water
MSL	Mean Sea Level
MSLP	Mean Sea Level Pressure
NASA	National Aeronautics and Space Administration
NAVD88	North American Vertical Datum of 1988
NIR	Near-infrared
NLG	Nelson Lagoon
NNK	Naknek
NOAA	National Oceanographic and Atmospheric Administration
NSF	National Science Foundation
NSM	Net Shoreline Movement
NWS	National Weather Service
OPUS	Online Positioning User Service
PDO	Pacific Decadal Oscillation
PDOP	Position Dilution of Precision
QAPP	Quality Assurance Project Plan
RGB	Red, Green, Blue
RMS	Root Mean Square
RSL	Relative Sea Level
RSLR	Relative Sea Level Rise
RSS	Root Sum Square
RTK	Real-time Kinematic

SECD	Strategic Economic and Community Development
SfM	Structure-from-Motion
SIFT	Scale-Invariant Feature Transform
SONAR	Sound Navigation and Ranging
SVTM	Single Value Threshold Map
TBC	Trimble Business Center
TIN	Triangulated Irregular Network
TWL	Total Water Level
UAV	Unmanned Aerial Vehicle
UNAVCO	University NAVSTAR Consortium
USACE	United States Army Corps of Engineers
USGS	United States Geologic Survey
WCI	Weighted Confidence Interval
WEAR	Waste Erosion Assessment and Review
WIS	Wave Information Study
WLR	Weighted Linear Regression Rate
WMO	World Meteorological Organization
WR2	Weighted R Squared

ACKNOWLEDGEMENTS

This research was funded by the Cooperative Institute for Alaska Research (CIFAR) as well as Alaska Sea Grant (ASG), with generous support from the National Science Foundation (NSF) (Grant # 1848542). I would like to thank Uma Bhatt, Nancy Fresco, and Sarah Garcia from CIFAR – their assistance allowed for the training I received from Deltares Institute as well the site visit to Nelson Lagoon in 2019. A special thank you to Ginny Eckart and Christina Sutton from ASG for their persistent support in enabling my research and education.

I would also like to thank the Nelson Lagoon Environmental Depart for their continued communication and assistance on the ground at Nelson Lagoon; thank you so much Mark McNeley, Angela “Angie” Johnson, and Samantha “Sam” McNeley. I greatly appreciate your help and look forward to our continued collaboration. Thank you to Jared Roberts for your work in 2018 collecting survey data in Nelson Lagoon. Thank you, Ronnie McPherson from HDR Alaska Inc., for taking time out of your busy schedule to talk with me and provide a trove a data from which I could build from. Thank you to Robin Bronen from Alaska Institute for Justice (AIJ) for initiating communication with the Native Village of Nelson Lagoon and moving forward efforts to monitor and record coastal change.

I would like to thank my advisor and committee chair, Dr. Chris Maio, whose unwavering work ethic, and passion for geoscience inspired me to pursue higher education. A big thank you to Dr. Daniel Mann. Your curiosity and discipline in learning has taught me what a true scientist looks like. I would also like to thank Jaci Overbeck; your steadfast dedication to quality and societal applicability has taught me perspective in the science world.

I have received help in various forms from many others over these last three years and am grateful to all of you; thank you Rich Buzard, Vladimir Alexeev, Shira Ellenson, Skye Hart, Harper Baldwin, and Autumn Fournier. I would also like to thank Paul McCarthy and Kinchel Doerner for their review of this document as well as their understanding and flexibility.

Finally, a heartfelt thank you to my parents. I am inspired by you; you have taught me attention to detail, self-honesty, and self-discipline. I promise to always bring pride to our name.

[This page is intentionally left blank]

PREVIEW

CHAPTER 1

INTRODUCTION

1.1 Introduction

Alaska has undergone substantial changes over the last few decades in various atmospheric and cryospheric systems and processes (Bader et al., 2011). Typical annual average statewide temperatures are now 3 to 4°F (~2 to 3°C) warmer than during the early and mid-20th century (Thoman and Walsh, 2019). This regional warming has been linked to increased storm frequency and intensity in the Bering Sea due, in part, to enhanced land-sea thermal contrast along the Arctic Frontal Zone (AFZ) (Zhang et al, 2004; Day and Hodges, 2018). This rapid Arctic warming relative to northern hemisphere mid-latitudes – referred to as Arctic Amplification (AA) – has been attributed to more frequent high-amplitude (wavy) jet-stream configurations, which also increases the frequency of extreme weather events (warm/cold snaps, storms, etc.) (Wallace and Hobbs, 1979; Francis and Vavrus, 2015). When combined with increased open water days due to the decline in sea-ice, this regime change has increased the occurrence of synchronous changes to shoreline morphology (Jones et al., 2009; Vermaire et al. 2013), rapid habitat degradation through salinization of freshwater and terrestrial ecosystems (Vermaire et al. 2013), and the destruction of infrastructure in coastal communities throughout the region (Graham and Diaz, 2001; Jones et al, 2009; Mesquita et al., 2010; Kinsman and DeRaps, 2012; Farquharson et al, 2018). These effects are especially relevant to Alaskan communities, since, as early as 2003, the United States General Accounting Office (GAO) reported that 184 out of 213 (86%) of Alaska Native villages are affected by flooding and erosion related hazards (GAO, 2003). Understanding the trends and dynamics of these changes along the Bering Sea coast is predicated on grasping both the spatial and temporal variability of storm climatologies in the North Pacific and Bering Sea (Atkinson, 2005; Rachold et al., 2005).

One such community located along the southern Bering Sea coastline is Nelson Lagoon (**Figure 1**), a native community of 50 people located on a narrow sand spit with no road connection to any other community. Essential infrastructure, such as freshwater resources and the airstrip, have

recently experienced substantial storm-driven erosion. The community lies at the historical southern limit of the open ocean sea-ice maximum and, starting over the last few decades, no longer experiences sea-ice each year (AOOS, 2014). This leaves the coastline without a natural barrier to blunt the impact of waves and surge for longer periods of time throughout the year (Vermaire et al. 2013). It also means surface winds have more contact with ocean water over larger areas for longer periods of time throughout the year, producing larger waves and surge (Erikson et al., 2015). This phenomenon has been quantified at St. Lawrence Island in the Bering Sea by Erikson et al. (2015), who found that the magnitude of surge events has increased over the last 30 years. Barrier beach systems are among the most dynamic of depositional coastal landforms and respond rapidly to changes in littoral sediment supply and sea level, as well as to the dynamic processes associated with severe storms including surge events (Mason and Jordan, 1993; Houser et al., 2008; Davidson-Arnott et al., 2019). This makes Nelson Lagoon and similar barrier beach systems that have likewise experienced modern declines in sea-ice extent and duration particularly useful as case studies to determine ramifications of the ongoing regime shift in the oceanographic and climatic conditions in the southern Bering Sea region.



Figure 1. Study site map of the Native Village of Nelson Lagoon. (A) UAV imagery over the residential portion of the community. The right side of the image is the Bering Sea, left side is the back-barrier lagoon. (B) Cross-shore image showing set-net cabin whose foundation has been undercut by storm-driven surge and wave action on the lagoon-side of the spit. (C) Regional map showing Nelson Lagoon's location on the North side of the Alaska Peninsula in Bristol Bay.

This project applies contemporary scientific tools combined with field investigations to determine Nelson Lagoon's vulnerability to flooding and erosion from future storm surge, as well as develop tools for mitigation applications (i.e. Smith, 2014).

1.2 Research Question and Objectives

This goal of this project is to identify spatial patterns of vulnerability to storm driven erosion and inundation at Nelson Lagoon through topographic analyses and by constructing a local hydrodynamic model set up for inclusion in a regional scale storm surge model. This goal was accomplished through the following objectives:

- 1) Conduct field investigations that include topographic, bathymetric, tide, and sediment surveys; compile climatic and oceanographic datasets.
- 2) Carry-out change analyses using remote sensing and surveyed datasets to quantify the extent and magnitude of shoreline change and flooding.
- 3) Construct a "seamless" topobathymetric elevation model and computational grid from existing and new survey data for inclusion in a regional storm surge model using Delft 3D FM.
- 4) Produce data products that inform community decision making and mitigation strategies.

1.3 Background

1.3.1 Regional Storm Regime

The center of a closed surface cyclonic circulation outside of the tropics is normally referred to as an extratropical cyclone (Jones et al., 2003; Bader et al., 2011). According to the Beaufort Wind Scale, an extratropical cyclone is categorized as a storm when the wind speed attains values greater than 24.5 m/s (55 mph) (WMO, 1970). Storms can last anywhere from 12 and 200 hours (up to >8 days), depending on the season and local geography and can vary in size from the mesoscale (≤ 1000 km) to synoptic scale (> 1000 km). Storms are often associated with damaging winds (Mesquita et al., 2009) and/or strong precipitation in the form of rain and snow and are an integral part of the atmospheric transport of heat, moisture (Sorteberg and Walsh, 2008), and momentum polewards (Yin, 2005; Bader et al., 2011).

While various analyses of storm activity have appeared in the literature, most have focused on the northern hemisphere as a whole, with the Arctic being treated separately in some instances (Keegan, 1958; Whittaker and Horn, 1984; Serreze, 1995; McCabe et al., 2001; Hoskins and Hodges, 2002; Zhang et al., 2004; Sorteberg and Walsh, 2008). Relatively few studies have focused on the North Pacific or Bering Sea region (Mason et al., 1996; Mesquita et al., 2009). This is a serious research gap because recent studies indicate that a warmer Arctic is accompanied by a northward shift in extratropical cyclone tracks (Geng and Sugi, 2003; Fischer-Bruns et al., 2005; Yin, 2005; Bengtsson et al., 2006; Rinke and Dethloff, 2008; Schuenemann and Cassano, 2010; Bader et al., 2011). The Northern Pacific/Bering Sea is one of the two main storm corridors in the Northern Hemisphere (**Figure 2**) (Hoskins and Hodges, 2002; Bernstein et al., 2008; Overland and Wang, 2019), mainly because of the geographical distribution of ocean and land in the Northern Hemisphere, which control the structure and magnitude of meridional temperature gradients (Rodionov et al., 2007).

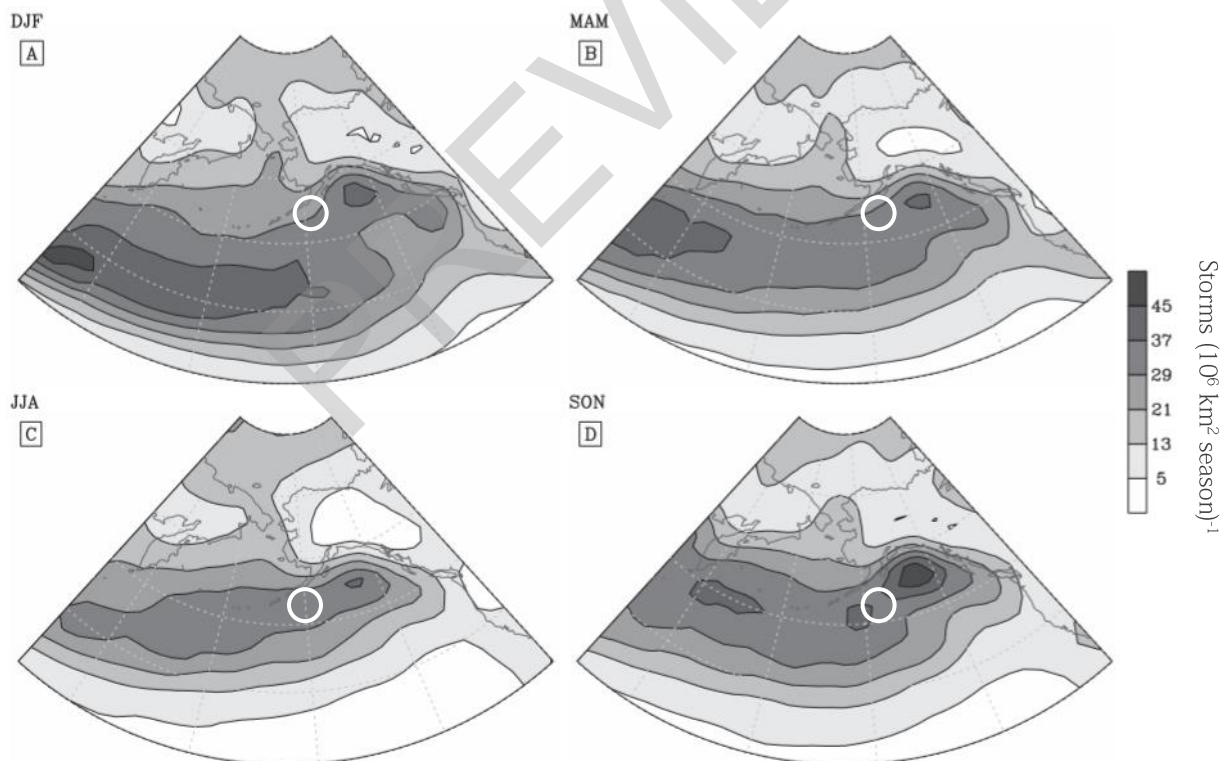


Figure 2. Storm track density climatology in the North Pacific from 1948/49 to 2008. (A) winter (DJF), (B) spring (MAM), (C) summer (JJA), and (D) autumn (SON) seasons. Units: Storms $(10^6 \text{ km}^2 \text{ season})^{-1}$. Location of Nelson Lagoon is noted by the white circles. Notice that Nelson Lagoon observes greater than 20 storms per season on average (after Mesquita et al., 2009).

The Bering Sea is characterized as an area of high lysis density (number of storms that dissipate within a defined region), especially during autumn and winter months (October – February); with winter storms being more intense (Cacchione and Drake, 1979; Overland and Pease, 1982; Sallenger et al., 1983; Mesquita et al., 2009). The principal influence on the Bering Sea surface is the Aleutian Low pressure cell (Mason et al., 1996; Rodionov et al., 2005). The Aleutian Low describes a statistical tendency toward low pressure associated with the passage of storms. One of the most widely used indices for the overall strength of the Aleutian Low is the North Pacific (NP) index (**Figure 3A**), which is related to the Pacific Decadal Oscillation (PDO) (**Figure 3B**) (Trenberth and Hurrell, 1994). When the NP index is positive it means that the Aleutian Low is relatively weak, and when it is negative the Aleutian Low is relatively strong. Rodionov et al. (2007) analyzed the NP index through time and found a correlation between negative NP index values and anomalously warm winters in the Bering region (**Figure 3C**). This occurs because the frequency of storms along the Alaskan track increases dramatically during the climate regimes of a strong Aleutian Low, increasing the overall probability of anomalously warm winters in the Bering Sea. As seen in Fig. 3A over the past 100+ years there were two multidecadal regimes of a strong Aleutian Low (1924–1946 and 1977–2005+) and two regimes of a weak Aleutian Low (1901–1923 and 1947–1976). The overall downward trend (increased storminess) in the NP index is noteworthy.

A study by Sepp and Jaagus (2011) found that the trend in the annual total number of cyclones in the Arctic increased by 55.8 cyclones over the period 1948–2002 and that the greatest increase in the frequency of cyclones was during the winter. There was a significant increase in the frequency of cyclones that specifically moved into the Arctic basin through the Bering Strait (Sepp and Jaagus, 2011). Moreover, the same study identified that the sea level pressure of Arctic cyclones showed a significant decreasing trend of 2.5 hPa (stronger storms) over the same study period.

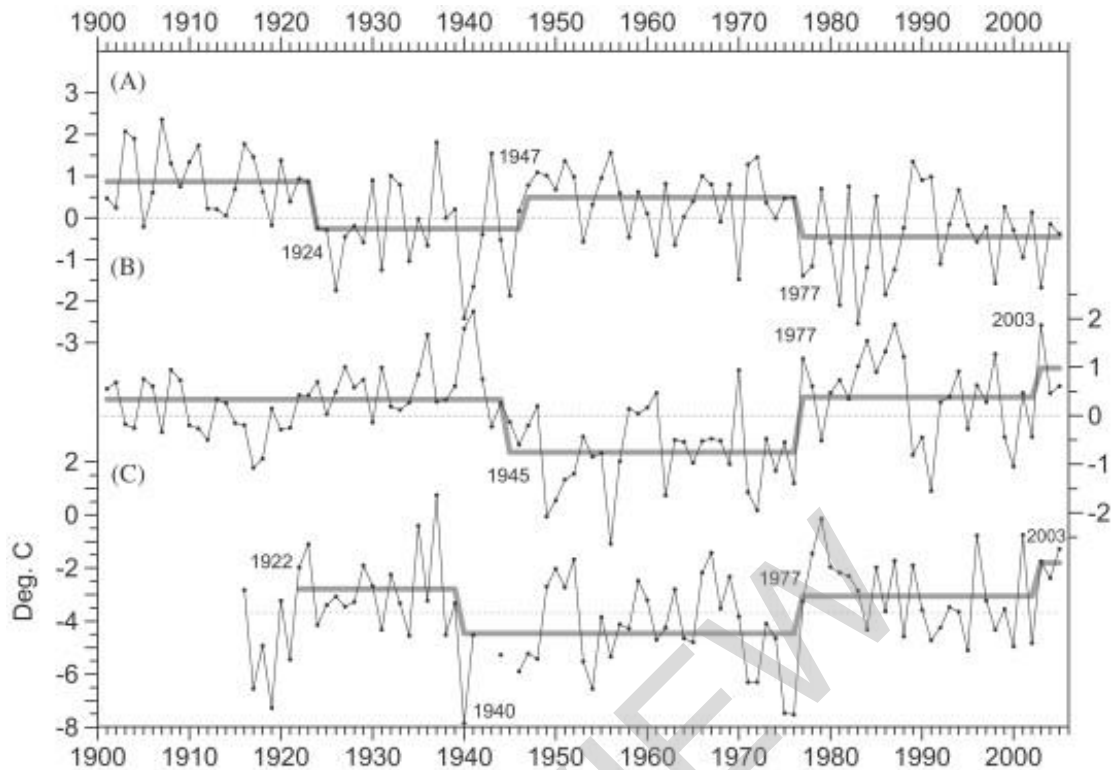


Figure 3. Plot showing the last hundred years of the mean winter (DJFM) North Pacific index, Pacific Decadal Oscillation Index, and surface air temperature in the Bering Sea. (A) North Pacific index, 1901–2005, unitless (B) Pacific Decadal Oscillation index, 1901–2005, unitless, and (C) surface air temperature in Celsius at St. Paul, 1916–2005. Bold gray lines characterize regime shifts calculated using the sequential method (from Rodionov et al., 2007).

1.3.2 Regional Sea Ice Regime

Sea-ice extent and duration strongly influence Arctic and Subarctic coastal dynamics, and changing climate is now altering the sea-ice regime of the Bering Sea (Farquharson et al., 2018). Open ocean sea-ice is an important moderator of wave fetch and water temperature, and shorefast sea-ice shields coastlines from wave action. Specifically, the extent of sea-ice has an inverse relationship with wave fetch, height, and swell size in Arctic seas (Stabeno et al., 2007; Francis et al., 2011; Overeem et al., 2011; Thomson and Rogers, 2014; Thomson et al., 2016), with the open-water season having the most wave energy available for coastal erosion and sediment transport (Overeem et al., 2011; Farquharson et al., 2018). Storms during the ice-free season generate the most geomorphologically significant wave events along Arctic coastlines and, hence, strongly influence coastal processes (Reimnitz et al., 1994; Mason et al., 1996; Forbes, 2011; Barnhart et al., 2014; Farquharson et al., 2018).

Winter ice formation in the Bering Sea has been described using the “conveyor belt” analogy (e.g., Muench and Ahlnas, 1976; Pease, 1980; Burns et al., 1981) in that sea-ice forms along the south facing coasts where polynyas (an open stretch of water) develop as the predominantly northerly winds carry sea-ice southward away from the coasts. Major polynyas occur south or down-wind of the Chukchi Peninsula, St. Lawrence and St. Matthew islands, and the Seward Peninsula. Sea-ice is then blown southward until it reaches warmer water where it melts, cooling the SST and allowing the ice edge to move southward (Stabeno et al., 1999; Stabeno et al., 2007; Danielson et al., 2011). In recent history, the southward edge seldom extended farther south than the deep water of the Aleutian basin south of the Bering Sea continental shelf (**Figure 1**).

The rate and dynamics of the sea-ice conveyor belt is strongly influenced by regional winds on a year-to-year basis (Zhang et al., 2010). Ice drift rates vary from 17 to 22 km/day to as fast as 28-32 km/day (Shapiro and Burns, 1975; Muench and Ahlnas, 1976; Weeks and Weller, 1984). In the Bering Strait, speeds as fast as 50 km/day have been observed, although there are reversals driven by wind events (Pease, 1980; Stabeno et al., 1999). Thus, the amount of ice moving south fluctuates considerably from year to year because of the substantial interannual variability of the winter northeasterly winds, which are linked to the location and intensity of the Siberian High and the Aleutian Low (Overland et al., 1999; Stabeno et al., 2001; Stabeno et al., 2007). The position of the mean ice edge during winter and early spring (January to April) is farthest south and relatively stable until April, after which the ice edge begins to retreat northward (Jones et al., 2020). By June, the ice edge has typically retreated northward through the Bering Strait, and by September, reaches its northernmost position off the continental shelf in the Chukchi and Beaufort Seas (Frey et al., 2015).

Over the past three decades, there have been significant changes in the timing and extent of sea-ice cover across the Bering, Chukchi, and Beaufort Seas (Jones et al., 2020). Satellite data reveal that patterns in sea-ice cover have been spatially heterogeneous through time, with significant declines of sea-ice extent in the Chukchi and Beaufort Seas, and complex multi-year variability in the Bering Sea south of St. Lawrence Island (**Figure 4**) (Frey et al., 2015). Stabeno et al. (2012) describe this multi-year variability in sea-ice cover over the southeastern Bering Sea shelf as involving oscillations between warm years (e.g., 2001–2005) with less extensive ice (driven

by weak, easterly winds) and cold years (e.g., 2007–2012) with more extensive ice (driven by cold, northerly winds). For example, the period 1979 to 2000 was characterized by high interannual variability in sea-ice, 2001 to 2005 was characterized by relatively low sea-ice cover, and 2006 to 2012 was characterized by relatively high sea-ice cover (AOOS, 2014; Frey et al., 2015). A weakened/wavy jet stream due to AA is associated with this increased variability in sea-ice cover across the Bering Sea (e.g., Wendler et al., 2014), a connection made evident by a shift from dominantly positive PDO values to more negative values over the last decade (Frey et al., 2015).

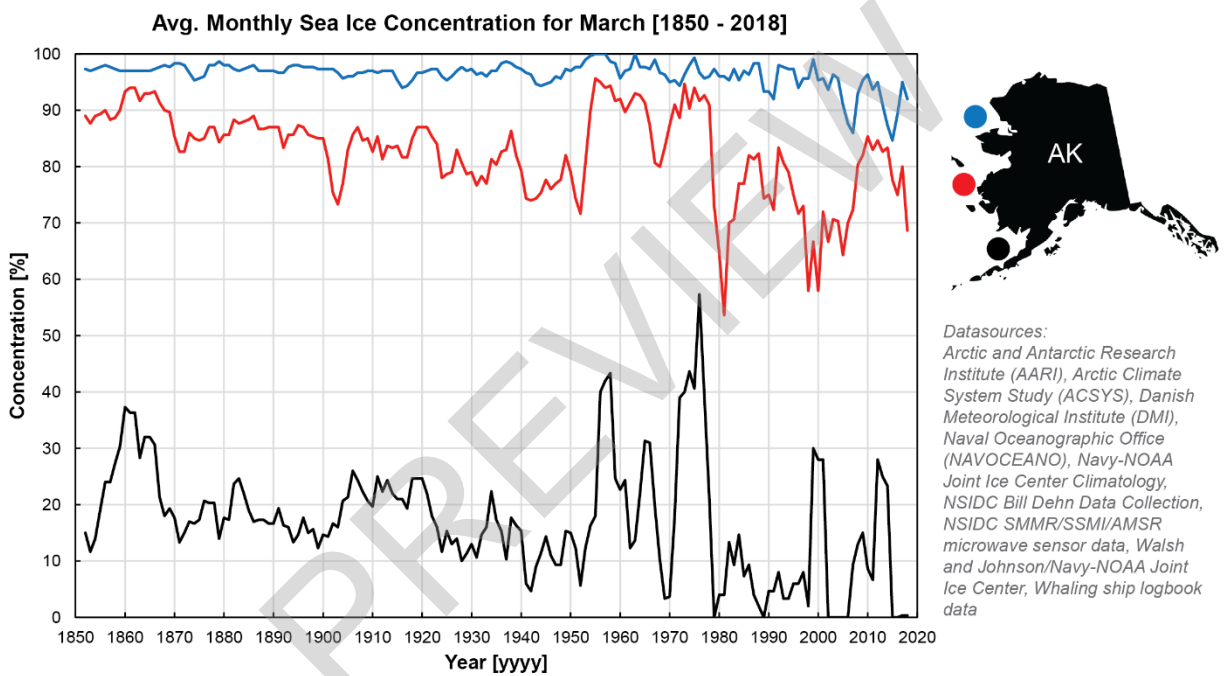


Figure 4. Megatransect of sea-ice concentrations for the month of March between 1850 and 2018 compiled from the Alaska Ocean Observatory Network (AOOS) Sea Ice Atlas. (0–30%) Open Water to very open drift, (30–90%) open drift to close pack, (90–100%) very close pack to compact. The black, red, and blue points in the upper right inset map correspond to the black, red, and blue sea-ice time series in the main graph. Notice how sea-ice in the Bering Sea (black) no longer consistently observe sea-ice each year (2000 onward).

The impacts of record low sea-ice extents in the Bering Sea since 2012 have been widespread and profound (Overland et al., 2011), including unprecedented weather events (Thoman et al., 2020), marine wildlife die-offs (Thoman et al., 2020), and sightings of animals outside of their normal range (Herring et al., 2018). Most pertinent to this project’s analysis of storm-driven